General Disclaimer

One or more of the Following Statements may affect this Document

- This document has been reproduced from the best copy furnished by the organizational source. It is being released in the interest of making available as much information as possible.

- This document may contain data, which exceeds the sheet parameters. It was furnished in this condition by the organizational source and is the best copy available.

- This document may contain tone-on-tone or color graphs, charts and/or pictures, which have been reproduced in black and white.

- This document is paginated as submitted by the original source.

- Portions of this document are not fully legible due to the historical nature of some of the material. However, it is the best reproduction available from the original submission.

NASA TECHNICAL MEMORANDUM

NASA TM-73872

NASA TM-73872

(NASA-TM-73872) THE INFLUENCE OF COMPOSITION, ANNEALING TREATMENT, AND TEXTURE ON THE FRACTURE TOUGHNESS OF Ti-5Al-2.5Sn PLATE AT CRYOGENIC TEMPERATURES (NASA) 46 p HC A03/MF A01 CSCL 11F G3/26

N78-15235

Unclas
57793

THE INFLUENCE OF COMPOSITION, ANNEALING TREATMENT, AND TEXTURE ON THE FRACTURE TOUGHNESS OF Ti-5Al-2.5Sn PLATE AT CRYOGENIC TEMPERATURES

by R. H. Van Stone, J. L. Shannon, Jr., W. S. Pierce, and J. R. Low, Jr.

TECHNICAL PAPER presented at the Symposium on Toughness and Fracture Behavior of Titanium sponsored by the American Society for Testing and Materials Toronto, Canada, May 2-3, 1977

THE INFLUENCE OF COMPOSITION, ANNEALING TREATMENT, AND TEXTURE ON THE FRACTURE TOUGHNESS OF Ti-5Al-2.5Sn PLATE AT CRYOGENIC TEMPERATURES

R.H. Van Stone[1], J.L. Shannon, Jr.[2], W.S. Pierce[2], and J.R. Low, Jr.[3]

MAY 1977

[1] Graduate Student, Department of Metallurgy and Materials Science, Carnegie-Mellon University; presently Metallurgist, General Electric Research and Development Center, Schenectady, New York 12301.

[2] Head and Engineer, respectively, Strength of Materials Section, NASA-Lewis Research Center, Cleveland, Ohio 44135.

[3] Professor, Department of Metallurgy and Materials Science, Carnegie-Mellon University, Pittsburgh, Pennsylvania 15213.

THE INFLUENCE OF COMPOSITION, ANNEALING TREATMENT, AND TEXTURE ON THE FRACTURE TOUGHNESS OF Ti-5Al-2.5Sn PLATE AT CRYOGENIC TEMPERATURES

R.H. Van Stone, J.L. Shannon, Jr., W.S. Pierce and J.R. Low, Jr.

ABSTRACT

The plane strain fracture toughness (K_{Ic}) and conventional tensile properties of two commercially produced one-inch thick Ti-5Al-2.5Sn plates were determined at cryogenic temperatures. One plate was extra-low interstitial (ELI) grade, the other normal interstitial. Portions of each plate were mill annealed at 1088°K (1500°F) followed by either air-cooling or furnace-cooling. The tensile properties, flow curves, and K_{Ic} of these plates were determined at 295°K (room temperature), 77°K (liquid nitrogen temperature), and 20°K (liquid hydrogen temperature).

The air-cooled ELI plate was the toughest material evaluated. K_{Ic} of the furnace-cooled ELI plate was about 25 percent below that of the air-cooled ELI material. Cooling rate from the annealing temperature had no influence on the toughness of the normal interstitial plates, both of which had a K_{Ic} approximately half that of the air-cooled ELI plate. The 20°K fracture toughness of the normal interstitial plates varied only slightly with specimen orientation. The LS toughness of both ELI plates was approximately 20 percent greater than the LT toughness.

Based on these results and a study of the microstructural fracture mechanism, it is recommended that Ti-5Al-2.5Sn which is to be used in applications requiring high fracture toughness have the lowest possible interstitial level and be air-cooled from the annealing treatment so as to prevent ordering.

KEY WORDS: Ti-5Al-2.5Sn, cryogenic temperatures, plane strain fracture toughness (K_{Ic}), microstructure, crystallographic texture, fracture

NOMENCLATURE

d_o = initial diameter of smooth tensile specimen

d = instantaneous diameter of smooth tensile specimen

A_o = original cross sectional area of smooth tensile specimen

A = instantaneous cross sectional area of smooth tensile specimen

a = instantaneous half-diameter of smooth tensile specimen necked region = $d/2$

R = radius of curvature of smooth tensile specimen necked region

e = conventional linear strain

P = load

σ_t = true stress

σ = Bridgman corrected flow stress

ε = true strain

P_{max} = maximum load in plane strain fracture toughness test

P_Q = secant offset load as defined in ASTM Method E-399-74

K_Q = provisional value of plane strain fracture toughness as defined in ASTM Method E-399-74

K_{Ic} = plane strain fracture toughness as defined by ASTM Method E-399-74

INTRODUCTION

The embrittling effects of increased levels of the interstitial elements (C, O, N, H) and substitutional iron, increased thickness, low test temperature, and slow cooling from the annealing treatment were first demonstrated for Ti-5Al-2.5Sn sheet in the early 1960's. Christian et al[1] observed decreases in mild-notch strength in liquid hydrogen (20°K)(-423°F) as alloy oxygen levels exceeded 0.1 wt-% and iron exceeded 0.25 wt-%. Broadwell and Wood[2] showed similar effects for sheet with 0.12 wt-% oxygen when the iron content exceeded 0.2 wt-%. These and similar studies resulted in the development of the ELI (extra low interstitial) grades of titanium alloys used today in applications where toughness is the limiting design consideration.

In 1963 Shannon and Brown[3] studied the effects of several alloy production and fabrication variables on sheet gages up to 0.25 in. at temperatures down to 20°K (-423°F) using sharp-notch tension specimens. Notch strength was reduced as temperature decreased, the effect being more pronounced the heavier the sheet gage. At 20°K (-423°F) the sharp-notch strength of normal interstitial sheet was half that of ELI grade. The so called plane-stress nominal fracture toughness, K_c, from the sharp-notched specimens of the air-cooled ELI sheet was 50% greater than furnace-cooled material, with no difference in smooth tensile strength. It was speculated that the precipitation of the ordered α_2 phase during slow furnace cooling was responsible for the lower toughness. These results are consistent with more recent work of Curtis, Boyer and Williams[4] which show reduced apparent toughness at room temperature for Ti-5Al-2.5Sn plate step-cooled from the annealing temperature compared to air-cooled plate. Attempts to detect α_2 precipitation using thin foil transmission electron microscopy in the lower toughness material were unsuccessful[4].

It has not been demonstrated that the effects observed for relatively thin gages of stock using sharp-notch strength or "plane-stress" fracture toughness are indicative of the behavior of heavy-section plane strain fracture toughness. The present investigation was therefore designed to examine the effects of interstitial level, annealing treatment cooling rate, and test temperature on the conventional smooth tensile properties and plane strain fracture toughness of heavy plate at temperatures down to 20°K (-423°F). In a companion study[5] the microstructure and fracture mechanism have been studied using fractographic and metallographic techniques. Those results are summarized here in an attempt to explain the observed trends in fracture toughness.

MATERIAL

Commercially available one-inch thick plate of Ti-5Al-2.5Sn alloy was investigated in four combinations of interstitial content and heat treatment: ELI and normal interstitial, either air cooled or furnace cooled from a 1088°K (1500°F) mill anneal. A single plate of each interstitial grade was subdivided for each of the two heat treatments. Chemical analyses of the as-received plates are given in Table 1 along with the specified compositions. It should be noted that in both the specified and analyzed compositions, higher iron contents accompany increased interstitial levels. In this paper the two investigated plate compositions are distinguished solely by the interstitial element level differences (ELI and Normal) as is customarily done by the titanium industry, notwithstanding the fact that some observed effects may be due to variations in iron content rather than interstitial content differences. The furnace cooling rate was essentially linear at approximately 15°K (27F°) per hour; air cooling rate was initially 4500K° (8100F°) per hour, with total cooling time to room temperature of about one hour.

Microstructures were examined with optical metallography, thin foil transmission electron microscopy (TEM), microprobe analysis, and texture pole figure determinations. The results are presented elsewhere[5] and are summarized in Table II. The α grain size of the furnace-cooled ELI plates was only slightly larger than the other plates. The iron-stabilized beta phase particle size and volume fraction was greater for the normal interstitial plate due to its higher iron content. The ELI plates had an annealed α deformation texture; the normal interstitial plates had a β deformation texture. Figure 1 shows a computer plotted pole figure of the basal (0002) and prism ($10\bar{1}0$) planes for the air-cooled ELI plate using the specimen and texture described by Olsen[6]. This texture is a typical annealed α deformation texture[7], with the basal planes parallel to the plate surface and split slightly toward the transverse direction. Figure 2 shows pole figures for the air-cooled normal interstitial plate. This is a β processing texture[7], with the basal planes perpendicular to the longitudinal and transverse directions. Figures 1 and 2 show that the prism planes are distributed in an almost random intensity. Although both plates were to have been identical except for interstitial and iron content, the differences in texture are most likely due to variations in processing[6]. Regardless of its source, the observed texture was quite mild for α titanium. Variations in cooling rate did not greatly alter the texture; however, it did affect the ordering characteristics of the α matrix. Figure 3 shows electron diffraction patterns of the α matrix of the air-cooled and furnace-cooled ELI plates with zone axes close to $(4\bar{5}15)$. The extra spots on the furnace-cooled pattern can be indexed as the ordered α_2 phase[8]. Similar patterns were obtained for the normal interstitial plates. Thus, the furnace-cooled plates were more ordered than the air-cooled plates.

PROCEDURE

The conventional tensile properties and plane strain fracture toughness (K_{Ic}) were determined for all plates at room temperature (295°K)(72°F), liquid nitrogen temperature (77°K)(-320°F), and liquid hydrogen temperature (20°K) (-423°F).[a] All cryogenic tests involved total immersion of the test specimen in cryogen.

All conventional tensile properties were determined for the longitudinal plate direction. Cylindrical specimens with 11.4 mm (0.45-in.) diameter by 101.6 mm (4-in.) long test sections were used at 20°K (-423°F); 6.4 mm (0.25-in.) diameter by 25.4 mm (1-in.) length at the other test temperatures. Load versus extension was autographically recorded up to maximum load for all smooth specimen tests at room temperature and 77°K (-320°F) using an LVDT-type extensometer. After maximum load, diametral strain was measured periodically by unloading and measuring specimen diameter at room temperature with a point micrometer. At 20°K (-423°F), strain was measured from two foil gages mounted 180° apart at specimen mid-length, and was recorded to just slightly beyond yield. Maximum and final loads were noted. From these measurements, Bridgman-corrected flow curves were constructed for all test temperatures by the procedure described in Appendix A.

Plane strain fracture toughness determinations were made for the LT orientation[9] at all three test temperatures, with additional LS orientation[9] tests at 20°K (-423°F). Standard compact specimens 25 mm (1-in.) thick were used at room temperature and 77°K. For these specimens, crack mouth opening displacement was measured using an LVDT clip gage developed by Shannon and Pierce[10]. The 20°K (-423°F) tests employed 25 mm (1-in.) thick three-point bend specimens. The LT specimens were 25 mm (1-in.) and 50 mm (2-in.) wide

(a) Tests at room temperature and 77°K (-320°F) were performed at Carnegie-Mellon University. The 20°K (-423°F) tests were conducted at NASA-Lewis Research Center.

and will be referred to as 1 x 1 and 1 x 2 bend specimens, respectively. The LS specimens were 1 x 1 bend specimens. Crack mouth opening displacement for the bend specimens was measured with a clip-in gage of the type described in ASTM Standard Method of Test E-399-74[9]. Special application of this gage to liquid hydrogen testing is described by Shannon, et al[11,12].

RESULTS

Strength and toughness. The conventional strength and plane strain fracture toughness results are summarized in Table III. Each value of mean and standard deviation is the result of triplicate tests at cryogenic temperatures, and duplicate tests at room temperature except as noted. All tests except those of the ELI plate at room temperature met the thickness and test record P_{max}/P_Q requirements of E-399-74[9]. Tests of the ELI plate at room temperature failed to meet the specimen thickness and test record P_{max}/P_Q requirements of E-399-74 and are properly noted as invalid in Table III.

Strength and LT toughness are displayed as a function of test temperature in Figure 4: 1 x 2 bend specimen results at 20°K (-423°F) compact specimen results at the higher temperatures. The error bars indicate the range of plus or minus one standard deviation. If they are not shown, the scatter falls within the datum point. As noted by Shannon and Brown[3], strength is essentially doubled as temperature is reduced from 295°K (room temperature) to 20°K (-423°F). The normal interstitial stock is 172 to 207 MM/m^2 (25 to 30 KSI) stronger than the ELI material at all test temperatures, and no influence of cooling rate from the annealing treatment is observed for either grade.

As expected, the ELI grade is substantially tougher than the normal interstitial grade. Cooling rate from the annealing treatment has no effect on the normal interstitial toughness, but at cryogenic temperatures the

air-cooled ELI grade toughness was 25 to 35 percent greater than that of the furnace-cooled ELI plate. Valid toughness of the ELI plate could not be measured at room temperature, but P_{max}/P_Q ratios from the test records suggest a similar effect at room temperature.

The 20°K toughness data are presented as bar graphs in Figure 5. Both the 1 x 1 and 1 x 2 LT bend specimens gave essentially the same results. This is not unexpected since 20°K fracture always occurred abruptly at maximum load before the 5% secant intersection.

Comparison of the LS and LT orientation fracture toughness specimens for the various alloy conditions reveals some plate directionality. LS toughness of the ELI grade is about 20% higher than the LT toughness. The toughness of the normal interstitial plates show little if any directionality.

Flow Curves. Tensile flow curves are shown in Figure 6. The datum points shown in that figure are the Bridgman-corrected[13] flow stress and the plastic strains as described in Appendix A. These data were fit using an iterative least square regression analysis to the form

$$\sigma = \sigma_o + A\varepsilon^m, \qquad \text{Equation (1)}$$

where σ_o, A and m are constants determined by a linear least square regression analysis with iteration on m to minimize the squared error. This form was chosen on the basis of its successful application to unalloyed titanium[14]. Table IV gives the values determined for the equation's constants. The fit of these curves is quite good: No experimental datum point was different from the regression stress by more than 3 percent.

Considerable license was taken in constructing the 20°K (-423°F) curves in Figure 6 which were based only on the yield and fracture events, and this

should be kept in mind when using those curves. The 20°K load-extension records were serrated and the specimens contained multiple necks, probably due to localized adiabatic heating during plastic deformation as described by Basinski[15]. The behavior is consistent with the observations of Kula and DeSisto[16] for unalloyed titanium at 4°K (-453°F) and of Carman and Katlin[17] for Ti-5Al-2.5Sn at 20°K (-423°F). Serrated yielding would not be expected to influence the flow curves developed for this test temperature, because it occurred outside the range where data was taken. Serrated yielding and multiple necking were not observed at the higher test temperatures, also consistent with Kula and DeSisto's[16] work.

Strain hardening rate as obtained by differentiating Equation 1,

$$\frac{d\sigma}{d\varepsilon} = m A\varepsilon^{m-1}, \qquad \text{Equation (2)}$$

is independent of σ_o. As shown in Figure 7, $d\sigma/d\varepsilon$ also appears independent of purity and cooling rate from the annealing treatment, and is influenced only by test temperature.

Due to the uncertainty in the 20°K (-423°F) flow curves at intermediate strains, the corresponding work hardening curves are not shown in Figure 7. Differences between the flow curves shown in Figure 6 for the two interstitial compositions results primarily from an increase in the apparent elastic limit (σ_o) with decreasing alloy purity. Similar observations have been made by Conrad et al[18] for unalloyed titanium.

Elastic modulus. Young's modulus was determined for the longitudinal plate direction from the load-extension records of triplicate tensile specimens tested at 20°K (-423°F) and from ultrasonic measurements on single specimens at room temperature[b]. These results are tabulated in Table V.

(b) Ultrasonic determinations of elastic moduli were made as a courtesy by Rockwell Science Center, Thousand Oaks, CA.

Crystallographic texture is known to influence the elastic properties of titanium. In unalloyed titanium, the elastic modulus normal to the basal plane is 45 percent greater than that in the basal plane[7]. Texture information (input to Figures 1 and 2) was combined with single crystal elastic constants to compute the room temperature elastic modulus of the Ti-5Al-2.5Sn plates using the computer program of Olsen and Moreen[19]. The predicted moduli trends mirror the measured values extremely well. The experimental data are approximately 10 percent high in every case, probably due to the stiffening influence of the alloying additions in the Ti-5Al-2.5Sn plates[20]. Agreement between the predicted and measured values suggests that the observed variations are due principally to crystallographic texture, rather than alloy purity or anneal cooling rate differences.

The computer-predicted room temperature moduli are shown as a function of in-plane orientation in Figure 8. The ELI plate had an annealed α-deformation texture: no basal planes were perpendicular to the longitudinal direction, but some split toward the transverse directions. Increasing the number of grains with basal planes perpendicular to the tensile axis increases the modulus, as shown in Figure 8. The normal interstitial plates had a β-processed texture. Basal planes were perpendicular to both the longitudinal and transverse plate directions, explaining the absence of a strong effect in Figure 8.

DISCUSSION

Strength and toughness variations with test temperature, alloy purity, and cooling rate from the annealing temperature observed in this study of 1-inch plate have confirmed earlier results by Shannon and Brown[3] for Ti-5Al-2.5Sn sheet. Decreasing test temperature and increasing interstitial and iron contents raise the strength and lower the toughness. Slow cooling from the annealing treatment reduces the toughness without affecting the strength of

the ELI grade stock, but does not affect the normal interstitial material. The influence of cooling rate for plate was as great as observed previously for sheet. Plate texture differences resulting from what were purported by the vendor to be identical processing and annealing schedules for the plate were perplexing, but their apparent effect on the elastic modulus and toughness directionality provided an interesting highlight to the study.

Fracture mechanism. Fractographic and metallographic sectioning studies have been conducted and reported upon separately[5]. Those results are drawn upon in this discussion to explain the observed trends in fracture toughness.

The in-depth metallurgical investigation was performed on specimens failed at 77°K (-320°F). Fractographic examination showed the fracture modes at 77°K (-320°F) and 20°K (-423°F) were identical, so it is assumed that metallurgical findings concerning fracture at 77°K (-320°F) apply equally to fracture at 20°K (-423°F). The fracture mode is dimpled rupture with a mixture of elongated and equiaxed dimples. Figure 9 shows a scanning electron microscope fractograph of a furnace-cooled ELI K_{Ic} specimen. The area shown is just ahead of the fatigue precrack. Crack propagation is from left to right. The elongated dimples form from cigar-shaped voids which nucleate at the intersections of localized shear deformation (slip bands or deformation twins) with grain boundaries or deformation twin boundaries. Figure 10 shows an optical micrograph of a region 45 μm below the fracture surface of an air-cooled ELI smooth tensile specimen tested at 77°K (-320°F). The fracture strain was 0.348. Two sets of parallel etched bands believed to be coarse slip bands intersect twin and grain boundaries forming offsets. Two voids indicated by arrows were observed at the offsets in a primary twin boundary. There is no void at the severe offset labelled A, indicating voids nucleate after offsets are formed.

The fracture process by nucleation, growth, and coalescence of cigar-shaped voids which produce elongated dimples on the fracture surface, is schematically illustrated in Figure 11. The process begins by the intersection of planar slip bands or deformation twins with twin or grain boundaries, as in Figure 11a. With increasing strain, offsets form in the boundaries at the end of the blocked shear bands, as in Figure 11b. The void nucleation event is characterized in Figure 11c by decohesion at the offset. The voids grow along the boundaries as in Figures 11d and 11e, and fracture occurs by void impingement and coalescence as in Figure 11f.

Some voids were observed to nucleate by decohesion at the interface of iron-stabilized β particles and the α matrix. This was observed frequently in the normal interstitial plates, but seldom in the ELI plates, most likely due to the smaller β particle size[21-23] of the low-iron ELI plates. This suggests that iron contents below 0.15 wt. % (level of the ELI plates in this investigation) will not produce further improvement in toughness.

Relation of Fracture Mechanism to Toughness

Factors influencing the toughness of Ti-5Al-2.5Sn alloy can be explained by the fracture mechanism. Of the events that lead to fracture (shown schematically in Figure 11), void nucleation is the most influential.[5] Factors which promote void nucleation decrease toughness. In the present study, reduced toughness correlated with an increased number and decreased size of elongated dimples on the fracture surface. Closely spaced dimples correspond to a higher rate of void nucleation which results in reduced dimple size, lessened energy expense in void growth, and consequently reduced toughness.

Voids were nucleated at the intersections of severe shear deformation bands (slip bands or deformation twins) with crystallographic boundaries (grain or twin boundaries), and at the interfaces between iron-stabilized beta

particles and the alpha matrix. Ninety percent of the voids in the ELI plates formed at blocked slip bands: for air cooled stock, predominately at primary twin boundary intersections; for furnace cooled stock, predominately at alpha grain boundary intersections. Void nucleation in the normal interstitial plates cooled at either rate was predominately by decohesion at the beta particle-matrix interfaces and at the intersections of multiple twins.

Void nucleation at blocked slip bands is controlled by the magnitude of stress concentration at the ends of the bands (where the voids form). The stress concentration is influenced by the distribution and length of the bands. The more coarse the slip band spacing (and hence the more dislocations or strain per slip band), and the longer the bands, the less macroscopic strain required for void formation. Previous investigations[24,25] have shown that reduced test temperature, increased interstitial level, and α_2 precipitation cause the character of slip in alpha titanium alloys to become planar and more coarse. In the present study, these were the observed embrittling factors.

Thin foil TEM revealed extremely coarse, planar slip bands for both air-cooled and furnace-cooled normal interstitial Ti-5Al-2.5Sn plates deformed at 77°K. In contrast, air-cooled ELI plate had planar, but relatively fine homogeneous slip bands. Furnace cooling the ELI plate produced coarsening to an intermediate degree, an effect owed to the ordering reaction evident in the diffraction patterns of Figure 3. The degree of slip coarsening correlated with the degree of embrittlement. The grain size of the plates was not a significant factor in this study because of its essential uniformity. It is tempting to speculate, however, that grain refinement might further improve the toughness of Ti-5Al-2.5Sn alloy through its effect of reducing the stress concentration at the ends of the foreshortened slip bands or deformation twins.

Texture and Directionality

The fracture toughness directionality (LT versus LS specimen crack-plane orientation) is believed due to the variation in crystallographic texture among the plates tested. To explain the observed trends, reference is made to an analysis of the resolved shear stresses for slip and for twinning in Appendix B.

The ELI plates possessed an annealed α-deformation texture. Void nucleation took place primarily at blocked slip bands. The analysis of Appendix B predicts slip at lower stress intensity levels for LT oriented specimens than for LS oriented specimens. Slip band dislocation densities and stress concentrations would therefore be expectedly higher in the LT specimens. Preferential twinning is predicted for LS specimens by the analysis for resolved shear stresses for twinning (Appendix B). A higher incidence of twin intersections would be anticipated, having the effect of shortening slip band length and thereby reducing slip band stress concentration. These anticipated behaviors are in agreement with the observed toughness superiority of LS oriented specimens.

The normal interstitial plates were β-processed textured. Void nucleation occurred at beta particles and at multiple twin intersections. Beta-particle decohesion would be expected to be independent of specimen orientation. Resolved shear stress analysis in Appendix B indicates that twinning occurs with near-equal ease on four of the five operative twin systems for both specimen orientations. An additional twin system is operative for LT specimens, which would increase, however slightly, void nucleation rate for the LT specimen orientation. This explains the absence of significant directionality in the normal interstitial plates, with a hint of LS toughness superiority.

CONCLUSIONS

The mechanical properties of Ti-5Al-2.5Sn plate were evaluated over the temperature range from ambient to 20°K (-423°F). Decreases in test temperature and an increase in interstitial level resulted in higher yield strength and decreased fracture toughness. Variation in cooling rate from the annealing temperature had no influence on strength or tensile ductility. The variation in cooling rate did not affect K_{Ic} of the normal interstitial plates, but K_{Ic} of the air-cooled ELI plate was 30 percent greater than that of the furnace-cooled ELI plate. The combination of specimen orientation and crystallographic texture cause variations in Young's modulus and K_{Ic}. LS orientation fracture toughness was 20 percent greater than LT K_{Ic} in the ELI plates, but the variations in the normal interstitial alloys were substantially less.

Fractography and metallographic sectioning were used to investigate the fracture mechanism. It was shown that the fracture mechanism is dimpled rupture where voids nucleate at the intersection of intense localized shear bands with crystallographic boundaries and at the interfaces between beta particles and the alpha matrix. Increasing interstitial content, decreasing test temperature, and ordering caused by furnace-cooling from the annealing temperature cause the slip band structure to become coarser. The higher strain per slip band increases the rate of void nucleation and as a result decreases fracture toughness. An analysis of the deformation systems active in the crack tip region in these textured plates was used to explain the variations in toughness with specimen orientation.

The results of this investigation suggest that the plane strain fracture toughness of Ti-5Al-2.5Sn alloy at cryogenic temperatures can be improved by having the lowest possible interstitial level, cooling rapidly from the annealing temperature to avoid ordering, and reducing the iron content to a

maximum of 0.15 percent. It was suggested that a reduction in α grain size and texture - stress state combinations which suppress multiple twinning may also improve K_{Ic}.

ACKNOWLEDGMENTS

The work was performed in part under National Aeronautics and Space Administration Grant NGR-39-087-047. The authors would like to thank W. F. Brown, Jr., and W. D. Klopp of that organization for their helpful support and comments. The authors also appreciated the help of J. C. Williams, formerly of Rockwell International Science Center and presently of Carnegie-Mellon University, for his assistance in the ultrasonic determinations of elastic modulus.

APPENDIX A

FLOW CURVE TECHNIQUES

Flow stress-true plastic strain curves were developed at all test temperatures by fitting an emperical flow curve equation to the experimental data.

At 20°K (-423°F), only information from the load-extension record and the fracture event were available. At the higher test temperatures, the load-extension record was supplemented with specimen diameter measurements taken periodically up to fracture.

Up to 0.1 strain where necking occurred, true stress and true strain were computed from the load-extension records using the classical relationships[26]:

$$\text{True stress} \quad (\sigma_t) = \frac{P}{A_o} (e + 1); \qquad \text{A-1}$$

$$\text{True strain} \quad (\varepsilon) = \ln (e + 1). \qquad \text{A-2}$$

Beyond 0.1 strain, diameter measurements were used to compute true stress directly as $\sigma_t = P/A$, and true strain from the relation:

$$\varepsilon = 2 \ln (d_o/d). \qquad \text{A-3}$$

True stress beyond maximum load was corrected for hydrostatic tension in the neck by multiplication with the Bridgman[13] correction factor:

$$F = 1/[(1 + 2R/a)\ln(1 + a/2R)]. \qquad \text{A-4}$$

For use in this expression, a/R values were determined from room temperature tensile specimens of air cooled Ti-5Al-2.5Sn plates. Neck diameter and curvature were measured over a range of strains on a 20X shadowgraph. The results are compared with Bridgman's data for steels[13] in Figure A-1. The scatter

for both sets of data is enormous. Nevertheless, a least-squares regression line was drawn through each set, indicating an appreciable difference between the two classes of materials.

The equation for the Ti-5Al-2.5Sn regression curve is

$$a/R = -0.072 + 0.589\ \varepsilon \qquad \text{A-5}$$

In the present study, a/R values were assumed independent of test temperature, interstitial level and cooling rate from the annealing treatment, and the values calculated from equation A-5 used for all flow stress corrections. When a/R was negative, which occurs at strains below 0.122, a Bridgman correction factor of unity was used.

APPENDIX B

CRACK TIP DEFORMATION MODE ANALYSIS

To examine the influence of texture and specimen orientation on K_{Ic}, a computer program similar to the one described by Thornburg[27] was written to describe the resolved shear stress on a given slip or twin system as a function of the position of the C-axis on a stereographic projection for an arbitrarily imposed stress state. The deformation systems included the four slip systems [prism, basal, pyramidal, and $\overrightarrow{c+a}$ $(10\bar{1}1)$] and five twin systems [$(10\bar{1}2)$, $(11\bar{2}1)$, $(11\bar{2}2)$, $(11\bar{2}3)$, and $(11\bar{2}4)$] known to operate at cryogenic temperatures in α titanium.

It was assumed that the criterion for deformation by slip is the critical resolved shear stress. The index used to evaluate the operation of a given slip system was the resolved shear stress divided by the critical resolved shear stress for that particular slip system. The critical resolved shear stresses determined by Paton, Baggerly, and Williams[25] for titanium - 6.6 percent aluminum crystals at 77°K (-320°F) were used for the normalization. The index used for the activation of twin systems was a resolved shear stress criterion. There is no established critical resolved shear stress for twinning; however in most cases, the twin system with the highest resolved shear stress is the first system to operate. Reed-Hill[28] has shown that in polycrystalline zirconium, the variation in number of twins for several twin systems is very similar in shape to the variation in the resolved shear stress. Thus, the resolved shear stress appears to be an adequate index to determine if a given twin system is operating.

To examine toughness variations between the LS and LT orientation fracture toughness specimens, a stress state typical of that ahead of a crack was used in the computer program. There are many elasto-plastic finite element calculations which show the variation of the stresses with position and work-hardening

characteristics. Rice and co-workers[29,30] have analyzed the crack tip stress fields of elastic-perfectly plastic (non work-hardening) material using both slip line field theory and finite element calculations. These stresses were normalized so that the maximum stress which is parallel to the applied load is equal to unity. The normalized stresses used to calculate the resolved shear stresses for the LS and LT orientation fracture toughness specimens are given in Table B-I. For both specimen orientations, the maximum stress acts in the longitudinal plate direction and is the same so that equivalent levels of K_I are being compared.

The stereographic projections in Figure B-1 show the variation in the resolved shear stresses for slip normalized by the critical resolved shear stress for LT and LS orientation fracture toughness specimens. Figure B-2 shows the resolved shear stress for twinning for the same stress states. Figure B-1 shows that for alloys with an annealed α deformation texture, specimens with an LT orientation will tend to deform by prism and pyramidal slip at a lower K_I level than specimens with an LS orientation, but higher K_I levels by basal slip. For both orientations, $\vec{c+a}$ slip seems to be fairly unlikely. Figure B-2 shows that the resolved shear stress for twinning in plates with an α annealing texture is fairly low except for $(11\bar{2}2)$ twinning. This twinning system is most likely to occur at lower K_I levels in the LS specimen than one with an LT orientation. Void nucleation in the ELI alloys occurs most frequently at the intersection of slip bands with twin boundaries or grain boundaries[5]. It is argued that a reduction in slip band length and a more even distribution of slip would delay void nucleation to higher strains and in turn improve K_{Ic}. Calculation of the resolved shear for slip for LS and LT fracture toughness specimens suggests that slip will occur at lower K_I levels in LT specimens than LS specimens. Thus, at the same K_I level, there will

probably be more dislocations per slip band in LT specimens. The higher resolved shear stress for twins in the LS specimens suggests that the LS orientation will have a higher twin volume fraction than the LT specimen. A higher twin volume fraction of the $(11\bar{2}2)$ twins will tend to reduce the slip band length. These factors suggest that the LS K_{Ic} value will be higher than that for LT specimens for alloys with an α annealing texture. This is consistent with the observed K_{Ic} values for the air-cooled and furnace-cooled ELI alloys.

The normal interstitial alloys have a β processed texture. The resolved shear stresses on twin systems shown in Figure B-2 suggests that $(10\bar{1}2)$, $(11\bar{2}1)$, $(11\bar{2}3)$, and $(11\bar{2}4)$ twins are equally likely to occur for both LS and LT specimens with a β processed texture. Twins of the $(11\bar{2}2)$ system may also occur for LT specimens. Void nucleation in the normal interstitial alloys occurred most frequently at multiple twin intersections[5]. The resolved shear stress data on the twin system suggests that twinning can occur on many twin systems for fracture toughness specimens with both LS and LT orientations. From this, one would expect that K_{Ic} would be similar for both orientations, as observed.

REFERENCES

1. J. L. Christian, A. Hurlich, J. E. Chafey, and J. F. Watson, Proc. ASTM, 63, 1963, p. 578.

2. R. G. Broadwell and R. A. Wood, Materials Research and Standards, 4, 1964, p. 549.

3. J. L. Shannon, Jr. and W. F. Brown, Jr., Proc. ASTM, 63, 1963, p. 809.

4. R. E. Curtis, R. R. Boyer, and J. C. Williams, Trans. ASM, 62, 1969, p. 457.

5. R. H. VanStone, J. R. Low, Jr., and J. L. Shannon, Jr., "The Fracture Mechanism of Ti-5Al-2.5Sn at Cryogenic Temperatures," to be published.

6. R. H. Olsen, Metallography, 5, 1972, p. 369.

7. F. Larson and A. Zarkades, "Properties of Textured Titanium Alloys," Metals and Ceramics Information Center, Report MCIC-74-20, Battelle Columbus Laboratories, Columbus, Ohio, June 1974.

8. M. J. Blackburn, Trans. AIME, 239, 1967, p. 1200.

9. "Standard Method of Test for Plane-Strain Fracture Toughness of Metallic Materials," ASTM Designation E399-74.

10. J. L. Shannon, Jr. and W. S. Pierce, "An LVDT-Type Displacement Gage for Plane Strain Fracture Toughness Tests in Liquid Hydrogen," to be published.

11. J. L. Shannon, Jr., R. T. Bubsey, and W. S. Pierce, "Plane Strain Fracture Toughness Assessment of Thick-Walled Liquid Hydrogen Transfer Pipe Made of Welded Centrifugally-Cast 21-6-9 Stainless Steel," to be published.

12. W. S. Pierce and J. L. Shannon, Jr., "Use of the ASTM E-399 Displacement Gage for Plane Strain Fracture Toughness Tests in Liquid Hydrogen," to be published.

13. P. W. Bridgman, Studies in Large Plastic Flow and Fracture, McGraw-Hill, New York, 1952.

14. S. N. Monterio and R. E. Reed-Hill, Met. Trans., 4, 1973, p. 1011.

15. Z. S. Basinski, Proc. Roy. Soc., London, A240, 1957, p. 229.

16. E. Kula and T. DeSisto, ASTM STP 387, 1966, p. 3.

17. C. M. Carman and J. M. Katlin, ASTM STP 432, 1968, p. 124.

18. H. Conrad, K. Okasaki, V. Gadgil, and M. Jon, Electron Microscopy and Structure of Materials, University of California Press, Berkeley, 1972, p. 438.

19. R. H. Olsen and H. A. Moreen, Met. Trans., 4, 1973, p. 701.

20. H. R. Ogden, D. J. Maykuth, W. L. Finlay, and R. I. Jaffee, Trans. AIME, 197, 1953, p. 267.

21. R. H. VanStone, R. H. Merchant, and J. R. Low, Jr., ASTM STP 556, 1974 p. 93.

22. T. B. Cox and J. R. Low, Jr., Met. Trans., 5, 1974, p. 1457.

23. M. A. Greenfield and H. Margolin, Met. Trans., 3, 1972, p. 2649.

24. N. E. Paton, J. C. Williams, and G. P. Rauscher, Titanium Science and Technology, Plenum Press, New York, 1973, p. 1049.

25. N. E. Paton, R. G. Baggerly, and J. C. Williams, "Deformation and Solid Solution Strengthening of Titanium Aluminum Single Crystals," Report SC 526.7FR, Rockwell International Science Center, January 20, 1976.

26. G. E. Dieter, Jr., Mechanical Metallurgy, McGraw-Hill, New York, 1961, p. 237.

27. D. A. Thornburg, "Cold-Rolling Texture Development in Titanium and Titanium-Aluminum Alloys," Ph.D. Thesis, Department of Metallurgy and Materials Science, Carnegie-Mellon University, 1972.

28. R. E. Reed-Hill, Deformation Twinning, Gordon and Breach, New York, 1964, p. 295.

29. J. R. Rice and C. F. Rosengren, J. Mech. Phy. Solids, 16, 1968, p. 1.

30. N. Levy, P. V. Marcal, W. J. Ostergren, and J. R. Rice, Int. J. Fracture Mech., 7, 1971, p. 143.

TABLE I

CHEMICAL ANALYSES OF Ti - 5 Al - 2.5 Sn PLATES
(Weight Percent)

	Al	Sn	Fe	Mn	O	C	N	H
ELI Specification	4.7/5.6	2.0/3.0	0.1/0.2	-----	0.12 Max	0.08 Max	0.05 Max	0.0125 Max
ELI, AC*	5.09	2.44	0.140	0.002	0.054	0.0057	0.0098	0.0056
ELI, FC †	5.10	2.47	0.145	0.002	0.052	0.0041	0.0098	0.0050
Normal Interstitial Specification	4.0/6.0	2.0/3.0	0.50 Max	0.30 Max	0.20 Max	0.15 Max	0.07 Max	0.003/0.020
Normal Interstitial AC*	5.22	2.47	0.300	0.002	0.164	0.0140	0.0163	0.0072
Normal Interstitial FC†	5.24	2.47	0.270	0.002	0.169	0.0120	0.0172	0.0042

* Air Cooled
† Furnace Cooled

TABLE II

Summary of Microstructure of Ti-5Al-2.5Sn Plates

Microstructural Feature	ELI		Normal Interstitial	
	AC*	FC†	AC*	FC†
α Grain Size (μm)	46.2	58.1	41.6	41.4
Estimated Size of Iron-Stabilized β Particles (μm)	2	2	5	5
Ordering	No	Yes	No	Yes
Type of Texture	α	α	β	β

* AC indicates air-cooled from mill anneal

† FC indicates furnace-cooled from mill anneal

TABLE III

Mechanical Properties of Ti-5Al-2.5Sn Plates

(Data indicates the mean ± one standard deviation)

Alloy	Test Temperature °K (°F)	σ_y 0.2% Yield Strength (ksi) (a)	Ultimate Tensile Strength (ksi) (a)	Tensile Fracture Strain	K_{Ic} (ksi/in.) (b)	K_{Ic} Specimen Orientation (e) and Type
Ti-5Al-2.5Sn	295 (72)	102.1 ± 0.8	110.2 ± 1.1	0.528 ± 0.012	107.9 (c,d)	LT-Compact
ELI	77 (-320)	171.4 ± 2.0	181.9 ± 0.6	0.407 ± 0.041	101.1 ± 4.4	LT-Compact
Air-Cooled	20 (-423)	189.0 ± 1.0	203.5 ± 0.8	0.254 ± 0.028	81.5 ± 4.5	LT-1x2 Bend
					82.7 ± 1.8	LT-1x1 Bend
					96.9 ± 4.5	LS-1x1 Bend
Ti-5Al-2.5Sn	295 (72)	98.9 ± 0.7	108.4 ± 0.4	0.512 ± 0.025	104.9 (c)	LT-Compact
ELI	77 (-320)	170.6 ± 0.5	180.5 ± 1.0	0.402 ± 0.024	75.1 ± 0.4	LT-Compact
Furnace-Cooled	20 (-423)	189.4 ± 0.3	204.7 ± 1.6	0.207 ± 0.043	64.0 ± 1.1	LT-1x2 Bend
					61.8 ± 2.2	LT-1x1 Bend
					73.4 ± 5.1	LS-1x1 Bend
Ti-5Al-2.5Sn	295 (72)	125.9 ± 0.5	133.8 ± 0.4	0.455 ± 0.040	65.4 ± 4.4	LT-Compact
Normal Interstitial	77 (-320)	194.5 ± 1.0	207.3 ± 1.1	0.317 ± 0.015	48.6 ± 1.3	LT-Compact
Air-Cooled	20 (-423)	215.4 ± 2.3	228.9 ± 0.1	0.209 ± 0.029	46.8 ± 1.0	LT-1x2 Bend
					46.0 ± 1.0	LT-1x1 Bend
					45.7 ± 0.4	LS-1x1 Bend
Ti-5Al-2.5Sn	295 (72)	127.9 ± 0.6	132.6 ± 0.6	0.328 ± 0.055	60.0 ± 1.3	LT-Compact
Normal Interstitial	77 (-320)	200.0 ± 0.5	209.9 ± 0.3	0.327 ± 0.034	52.5 ± 1.8	LT-Compact
Furnace-Cooled	20 (-423)	220.3 ± 1.7	228.7 ± 0.4	0.124 ± 0.051	46.2 ± 0.2	LT-1x2 Bend
					42.7 ± 0.3	LT-1x1 Bend
					47.8 ± 3.3	LS-1x1 Bend

(a) 1 ksi = 7.9 MN/m^2

(b) 1 ksi/in = 1.1 $MN/m^{3/2}$

(c) This result is invalid because specimen thickness is less than 2.5 $(K_{Ic}/\sigma_y)^2$. Only one test was conducted.

(d) This result is invalid because P_{max}/P_Q exceeds 1.1.

(e) Orientation notation is that of ASTM E399-74.

TABLE IV

Flow Curves of Ti-5Al-2.5Sn Plate Fit to the Form $\sigma = \sigma_o + A\varepsilon^m$

Alloy	Test Temperature °K (°F)	σ_o (ksi) (a)	A (ksi) (a)	m
Ti-5Al-2.5Sn	295 (72)	98.0	77.5	0.50
ELI	77 (-320)	166.3	115.8	0.52
Air-Cooled	20 (-423)	172.5	135.6	0.35
Ti-5Al-2.5Sn	295 (72)	96.4	81.5	0.54
ELI	77 (-320)	165.9	121.3	0.55
Furnace-Cooled	20 (-423)	171.2	132.4	0.35
Ti-5Al-2.5Sn	295 (72)	120.5	82.9	0.47
Normal Interstitial	77 (-320)	180.3	129.2	0.40
Air-Cooled	20 (-423)	185.8	140.1	0.26
Ti-5Al-2.5Sn	295 (72)	123.4	81.2	0.55
Normal Interstitial	77 (-320)	189.9	127.5	0.46
Furnace-Cooled	20 (-423)	185.8	116.7	0.21

(a) 1 ksi = 6.9 MN/m^2

TABLE V

Longitudinal Young's Modulus (E) of Ti-5Al-2.5Sn Plates

	E at 20°K (-423°F)[a] (10^6 psi)[d]	E at 295°K (Room Temp.)[b] (10^6 psi)	Predicted[c] E at 295°K (Room Temp.) (10^6 psi)
ELI, Air-Cooled	18.1 ± 0.1	16.8	15.3
ELI, Furnace-Cooled	18.4 ± 0.1	16.9	15.2
Normal Interstitial, Air-Cooled	19.2 ± 0.1	18.0	16.1
Normal Interstitial, Furnace-Cooled	19.4 ± 0.1	18.0	19.1

(a) Determined from tensile specimen loud-extension records. Error limits represent range of 68 percent confidence limits.

(b) Determined using ultrasonic techniques.

(c) Predicted by computer program of Olsen and Moreen[19]

(d) 10^6 psi = 6900 MN/m^2

TABLE B-1

Normalized Stresses used for Calculation of the Resolved Shear Stresses for LS and LT Orientation Fracture Toughness Specimens

Stress Axis	LT Specimen	LS Specimen
Longitudinal	1.000	1.000
Transverse	0.607	0.804
Short-Transverse	0.804	0.607

FIGURE CAPTIONS

Figure 1: Texture Pole Figure of Air-Cooled ELI Ti-5Al-2.5Sn Plate. L, T, and S indicate longitudinal, transverse, and short transverse directions, respectively.

Figure 2: Texture Pole Figure of Air-Cooled Normal Interstitial Ti-5Al-2.5Sn Plate. L, T, and S indicate longitudinal, transverse, and short transverse directions, respectively.

Figure 3: Electron Diffraction Patterns of (a) Air-Cooled and (b) Furnace-Cooled ELI Ti-5Al-2.5Sn Plates having a $(4\bar{5}15)$ zone axis.

Figure 4: The Variation of Longitudinal Tensile Properties and LT Fracture Toughness of Ti-5Al-2.5Sn with Test Temperature. The error bars indicate the range of plus and minus one standard deviation.

Figure 5: Directionality of plates investigated as indicated by 20°K plane strain fracture toughness.

Figure 6: Tensile flow curves for Ti-5Al-2.5Sn.

Figure 7: Variation of the Work-Hardening Rate ($\partial\sigma/\partial\varepsilon$) of Ti-5Al-2.5Sn with Plastic Strain and Test Temperature.

Figure 8: Predicted Room Temperature Young's Modulus of the Ti-5Al-2.5Sn Plates as a Function of Orientation.

Figure 9: SEM Fractograph of a Furnace-Cooled ELI Ti-5Al-2.5Sn Fracture Toughness Specimen Tested at 77°K. The direction of crack propagation is from left to right. Regions "A" and "B" contain elongated and equiaxed dimples respectively.

Figure 10: Offsets and Void Nucleation Along Primary Twin Boundaries in an Optical Micrograph of a Sectioned Air-Cooled ELI Ti-5Al-2.5Sn Tensile Specimen Strained to 0.348 at 77°K. The arrows point to voids along the primary twin boundary at offsets. The letter "A" indicates an offset without void nucleation. The tensile axis is vertical.

Figure 11: Schematic of the Sequence of Events During Fracture by Cigar-Shaped Voids Forming Elongated Dimples.

Figure A-1: Comparison of room temperature a/R values as a function of strain for air cooled Ti-5Al-2.5Sn plates with those for Bridgman's Steels.[13]

Figure B-1: Stereographic Projections Showing the Variation of Normalized Resolved Shear Stress for Slip in LS and LT Orientation Fracture Toughness Specimens. L, T, and S indicate longitudinal, transverse, and short transverse plate directions, respectively.

Figure B-2: Stereographic Projections Showing the Variation of Resolved Shear Stress for Twinning in LS and LT Orientation Fracture Toughness Specimens. L, T, and S indicate longitudinal, transverse, and short transverse plate directions, respectively.

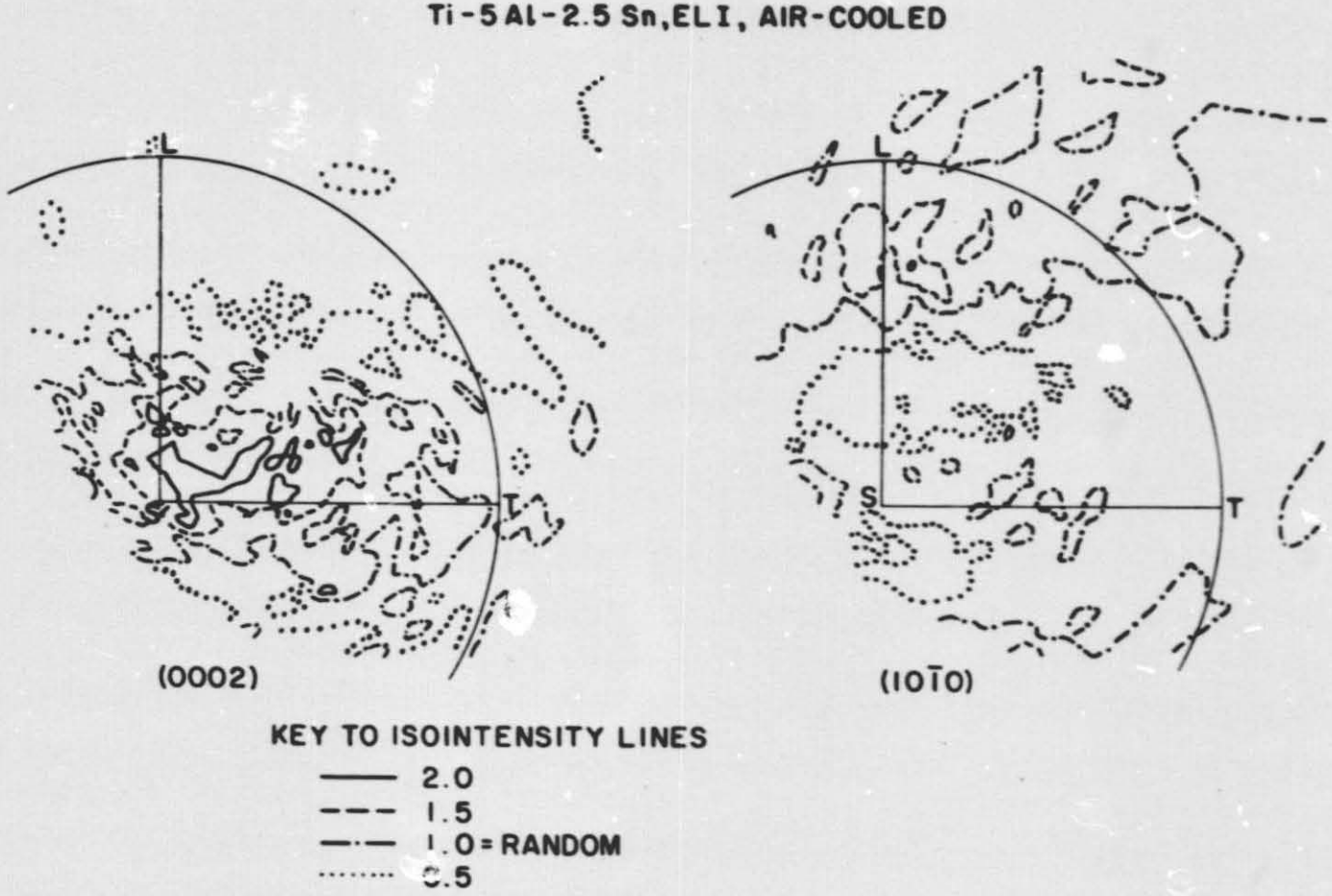

Figure 1. Texture Pole Figure of Air-Cooled ELI Ti-5Al-2.5Sn Plate. L, T, and S indicate longitudinal, transverse, and short transverse directions, respectively.

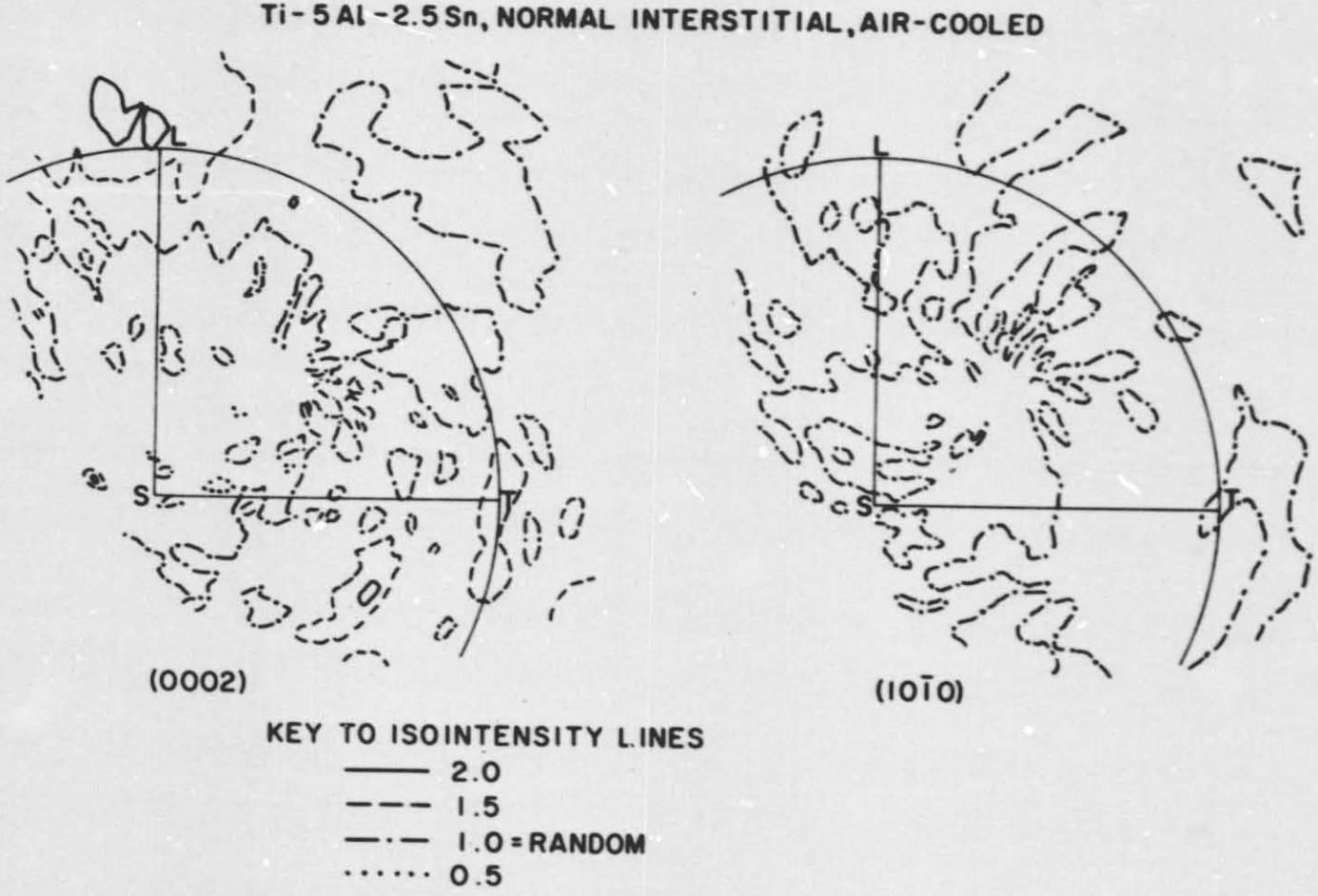

Figure 2. Texture Pole Figure of Air-Cooled Normal Interstitial Ti-5Al-2.5Sn Plate. L, T, and S indicate longitudinal, transverse, and short transverse directions, respectively.

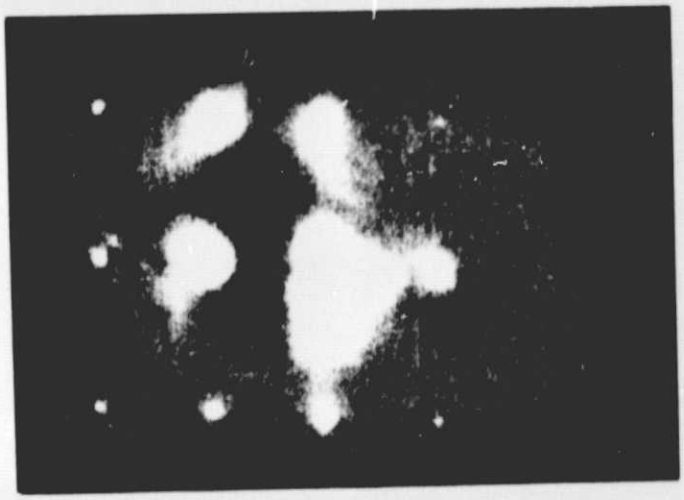

(a) Air-Cooled

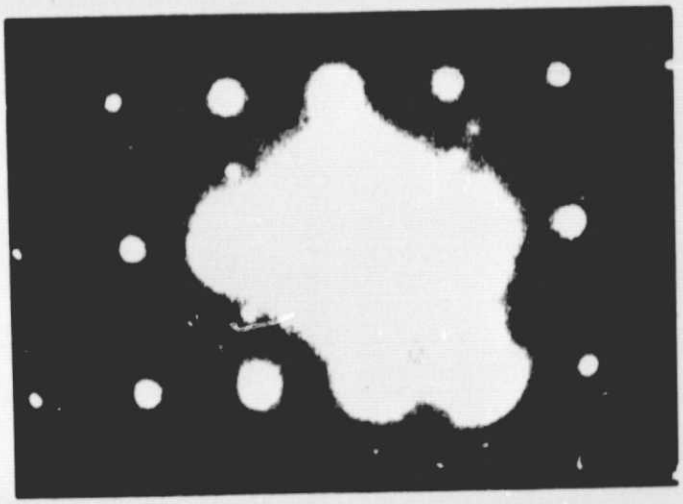

(b) Furnace-Cooled

Figure 3: Electron Diffraction Patterns of (a) Air-Cooled and (b) Furnace-Cooled ELI Ti-5Al-2.5Sn Plates having a (4$\bar{5}$15) zone axis.

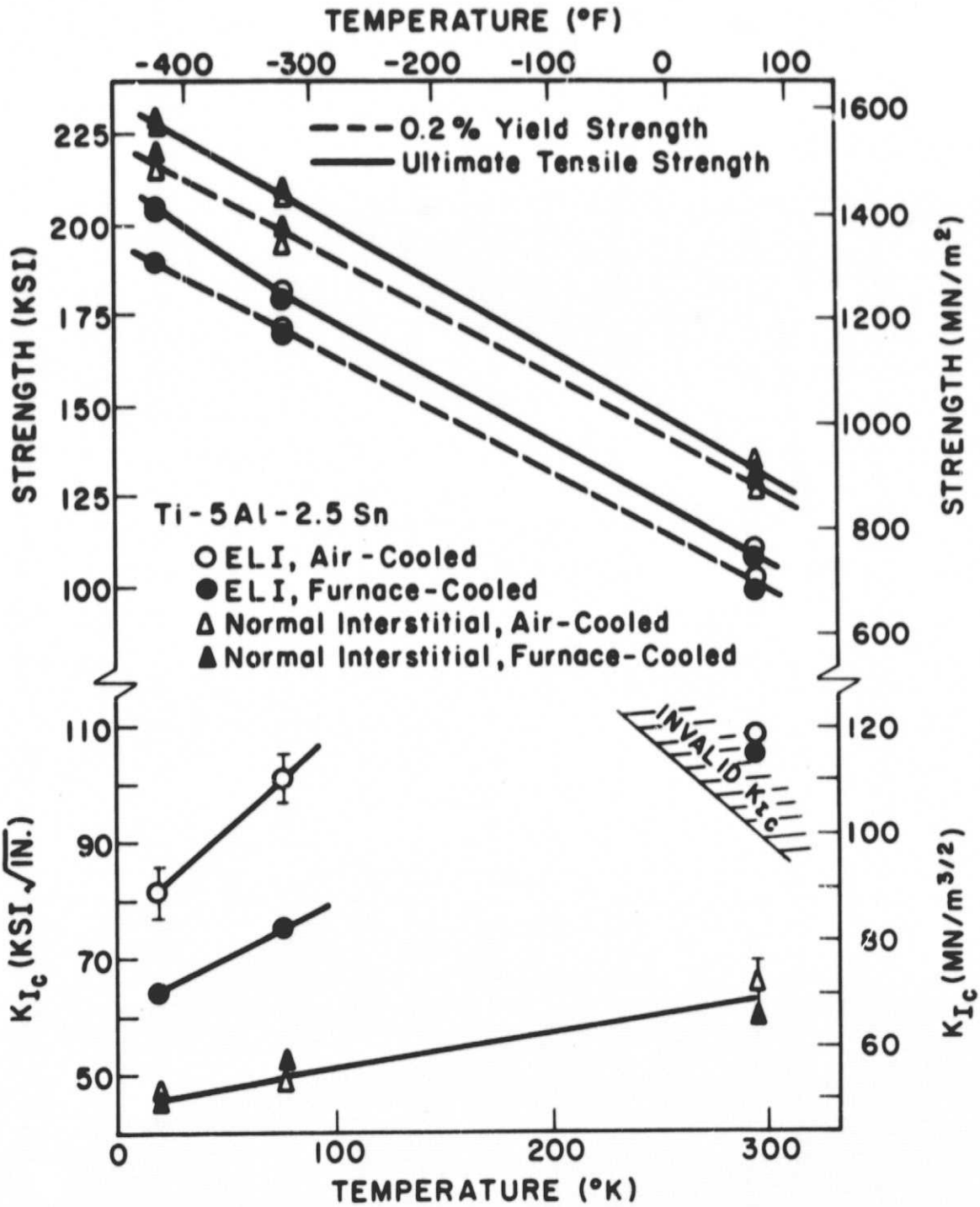

Figure 4. The Variation of Longitudinal Tensile Properties and LT Fracture Toughness of Ti-5Al-2.5Sn with Test Temperature. The error bars indicate the range of plus and minus one standard deviation.

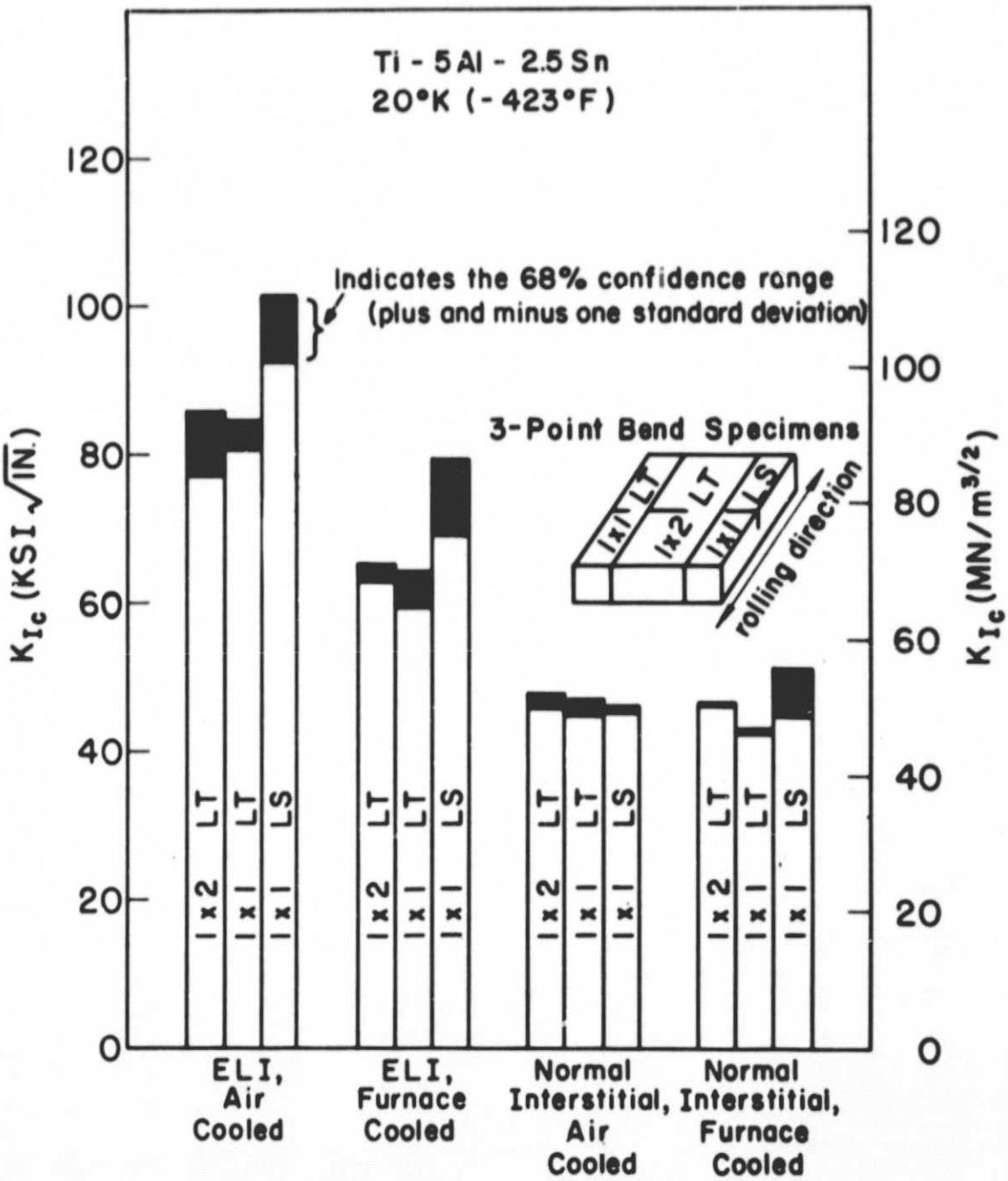

Figure 5: Directionality of plates investigated as indicated by 20°K plane strain fracture toughness.

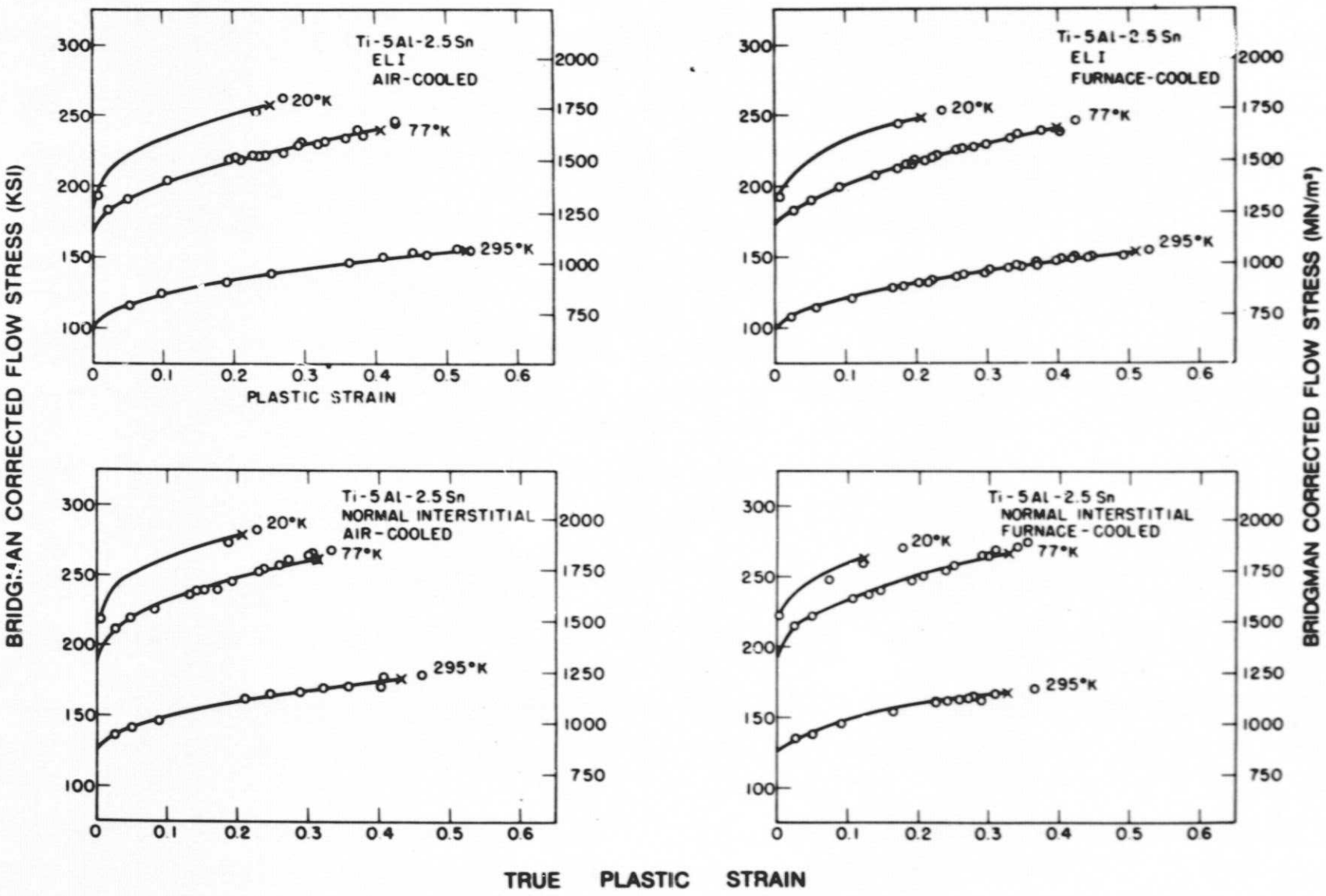

Figure 6: Tensile flow curves for Ti-5Al-2.5Sn.

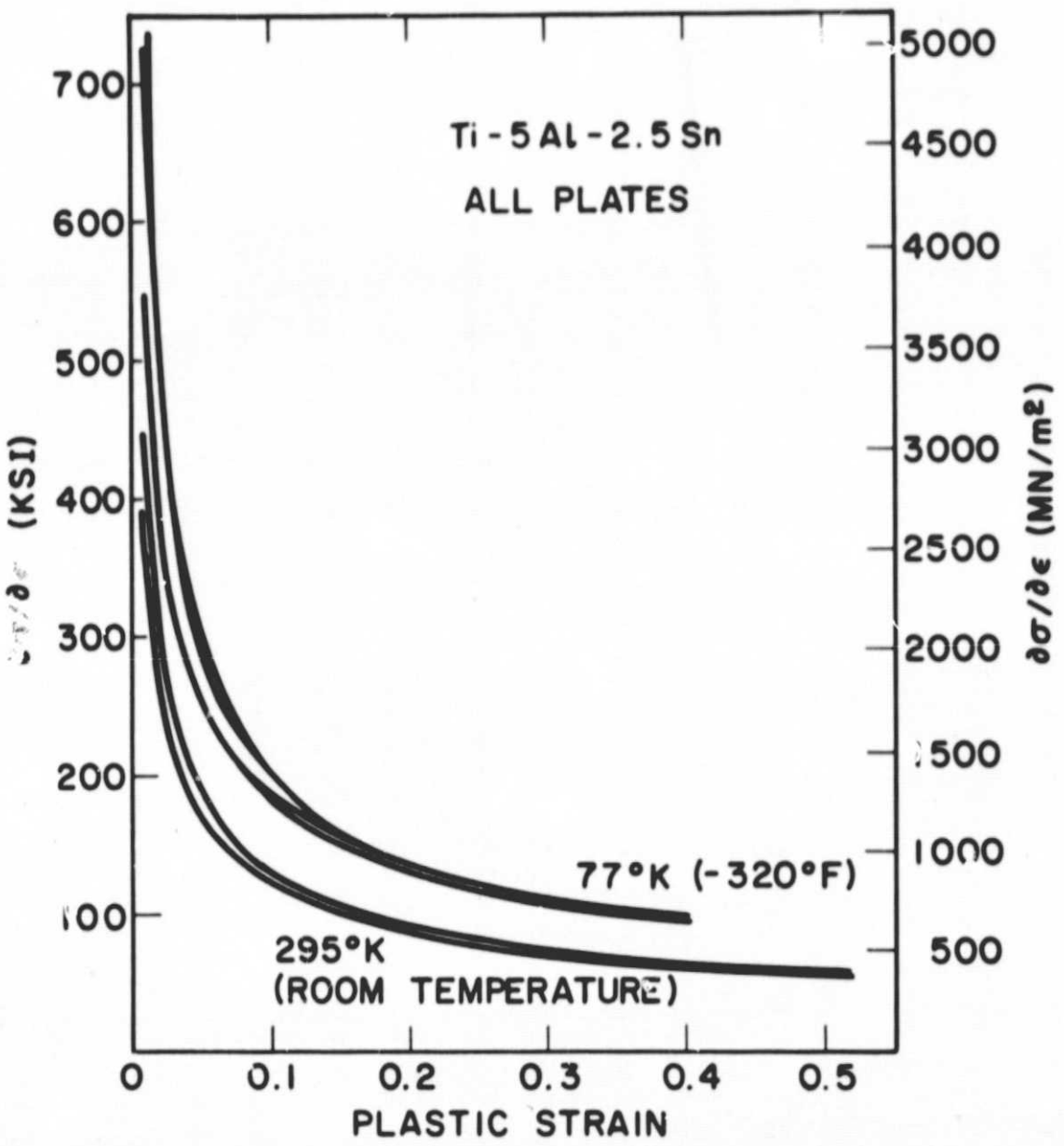

Figure 7: Variation of the Work-Hardening Rate ($\partial\sigma/\partial\varepsilon$) of Ti-5Al-2.5Sn with Plastic Strain and Test Temperature.

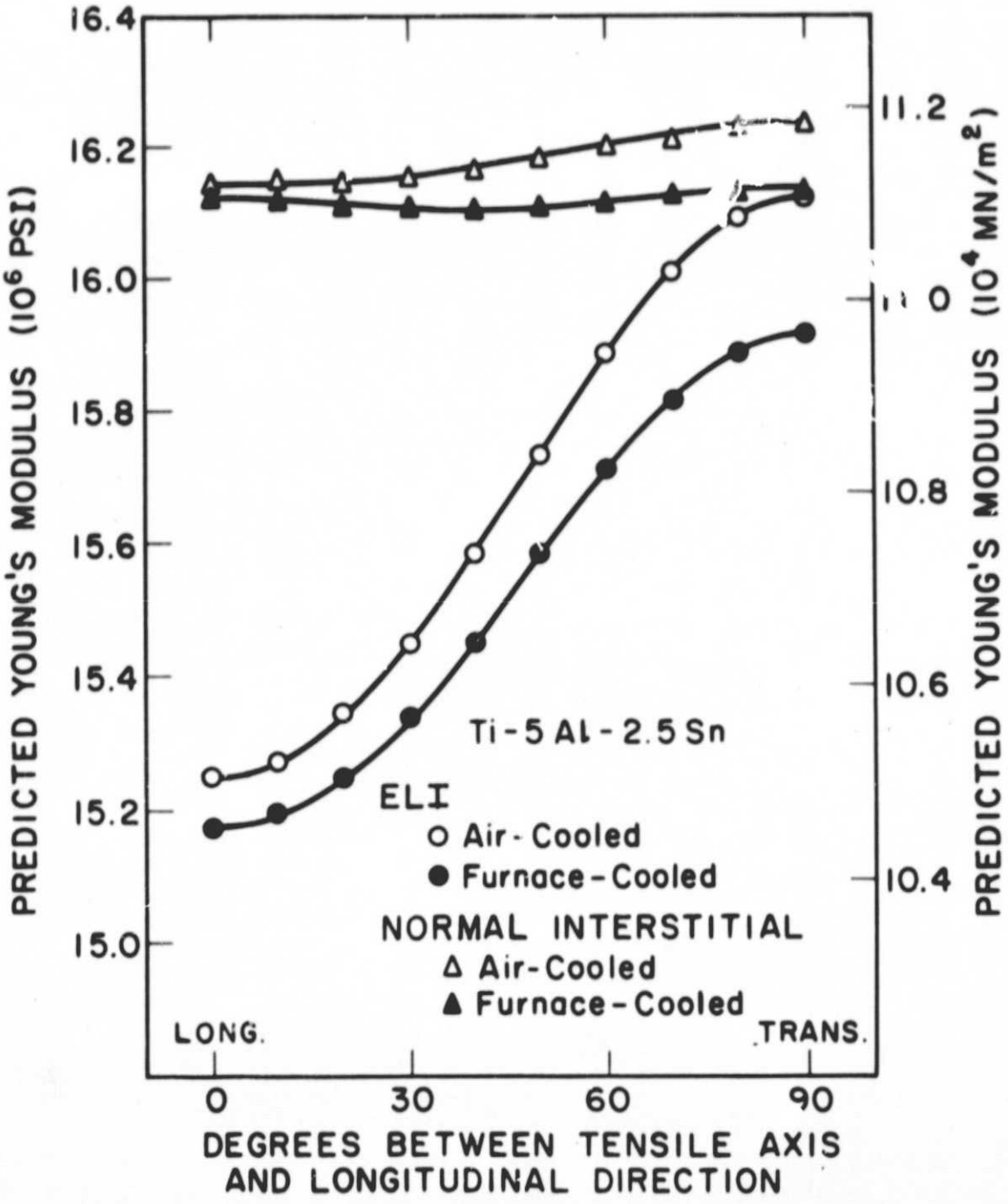

Figure 8. Predicted Room Temperature Young's Modulus of the Ti-5Al-2.5Sn Plates as a Function of Orientation.

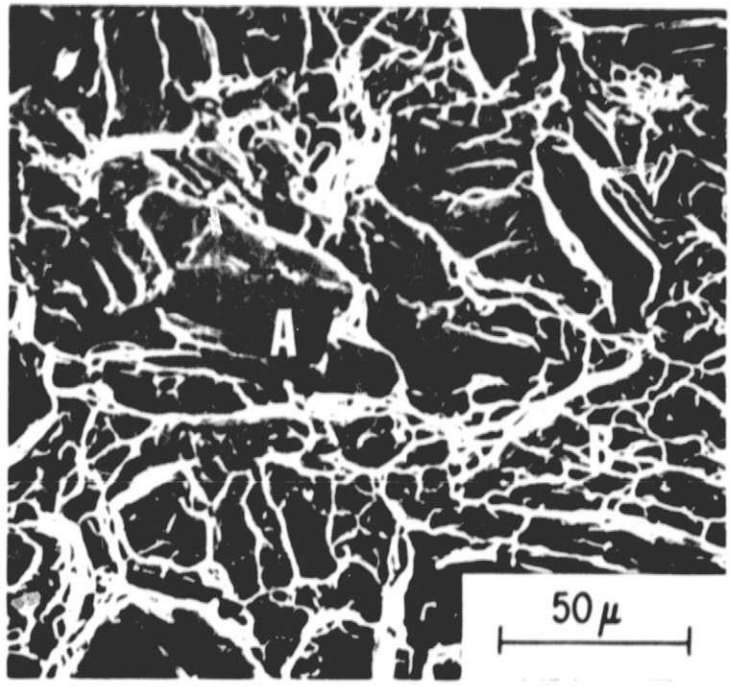

Figure 9. SEM Fractograph of a Furnace-Cooled ELI Ti-5Al-2.5Sn Fracture Toughness Specimen Tested at 77°K. The direction of crack propagation is from left to right. Regions "A" and "B" contain Elongated and Equiaxed Dimples Respectively.

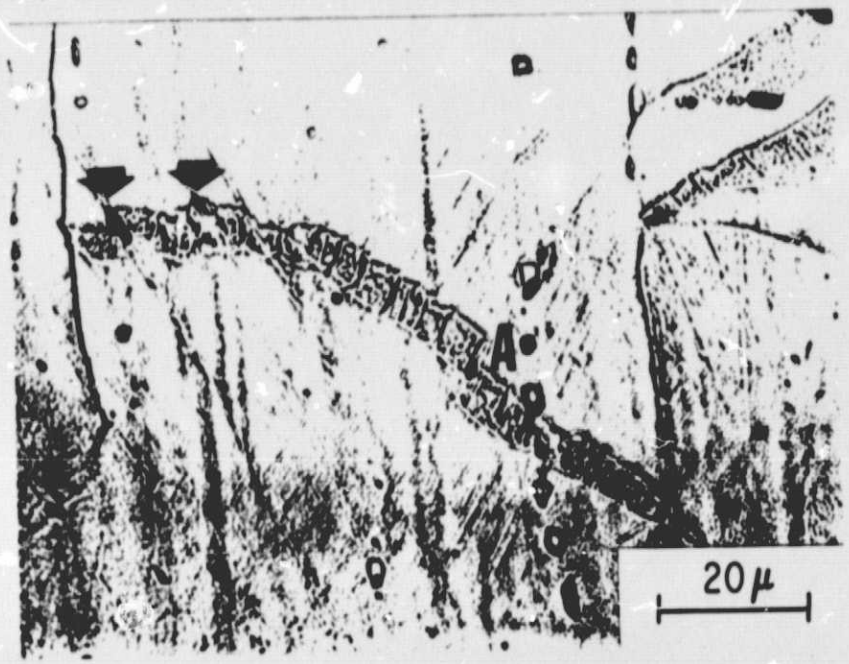

Figure 10. Offsets and Void Nucleation Along Primary Twin Boundaries in an Optical Micrograph of a Sectioned Air-Cooled ELI Ti-5Al-2.5Sn Tensile Specimen Strained to 0.348 at 77°K. The arrows point to voids along the primary twin boundary at offsets. The letter "A" indicates an offset without void nucleation. The tensile axis is vertical.

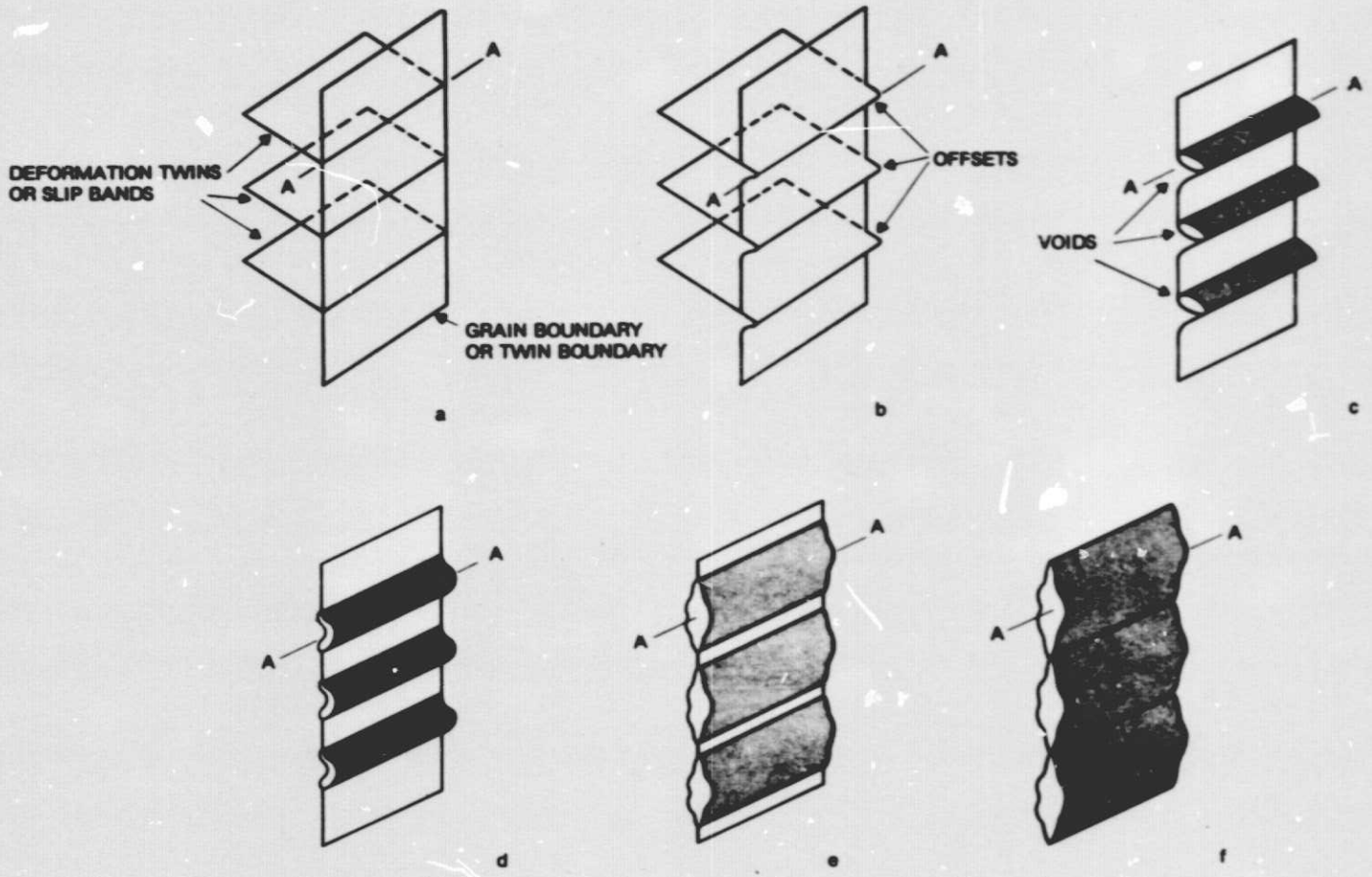

Figure 11: Schematic of the Sequence of Events During Fracture by Cigar-Shaped Voids Forming Elongated Dimples.

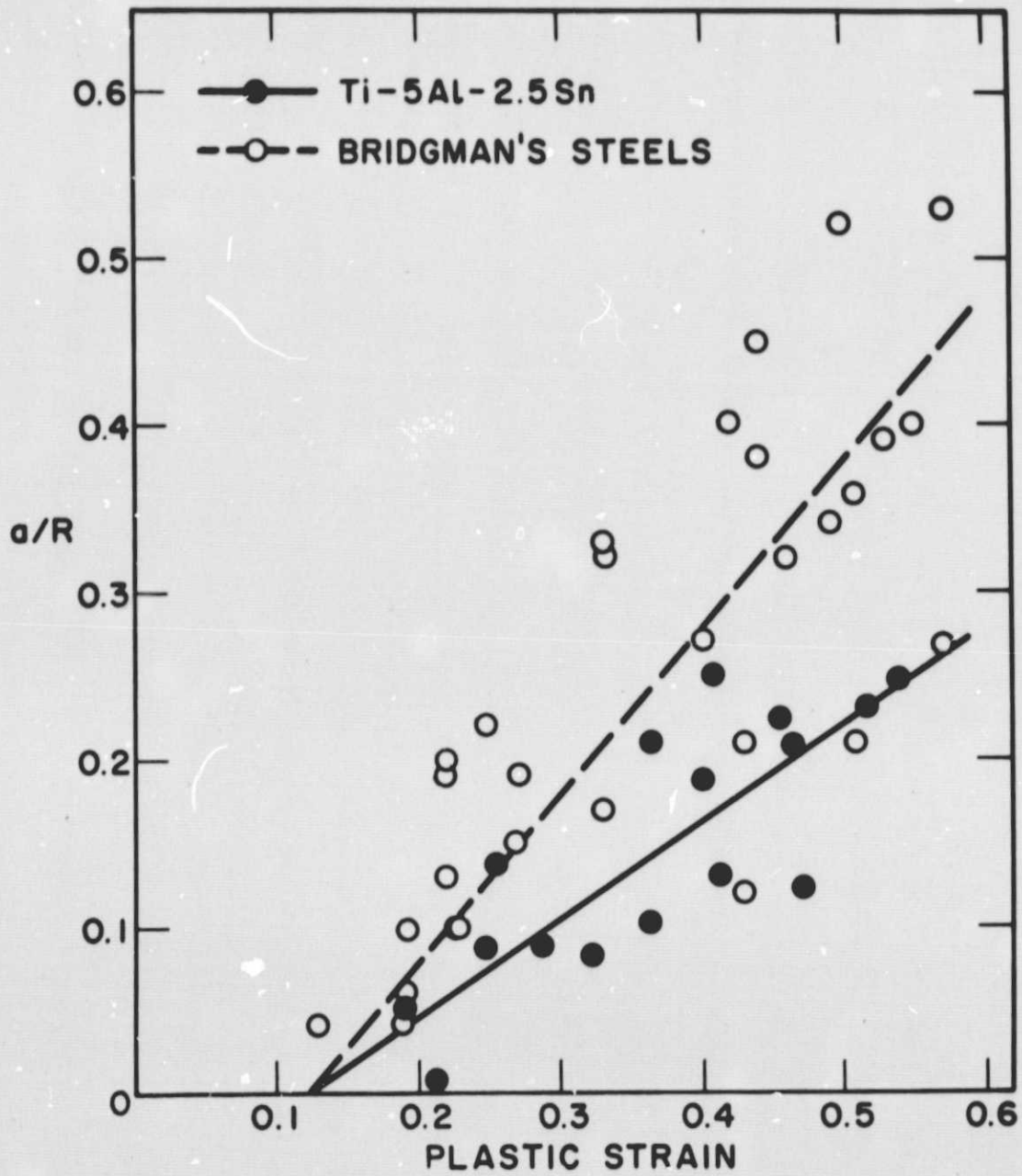

Figure A-1: Comparison of room temperature a/R values as a function of strain for air cooled Ti-5Al-2.5Sn plates with those for Bridgman's Steels. (13)

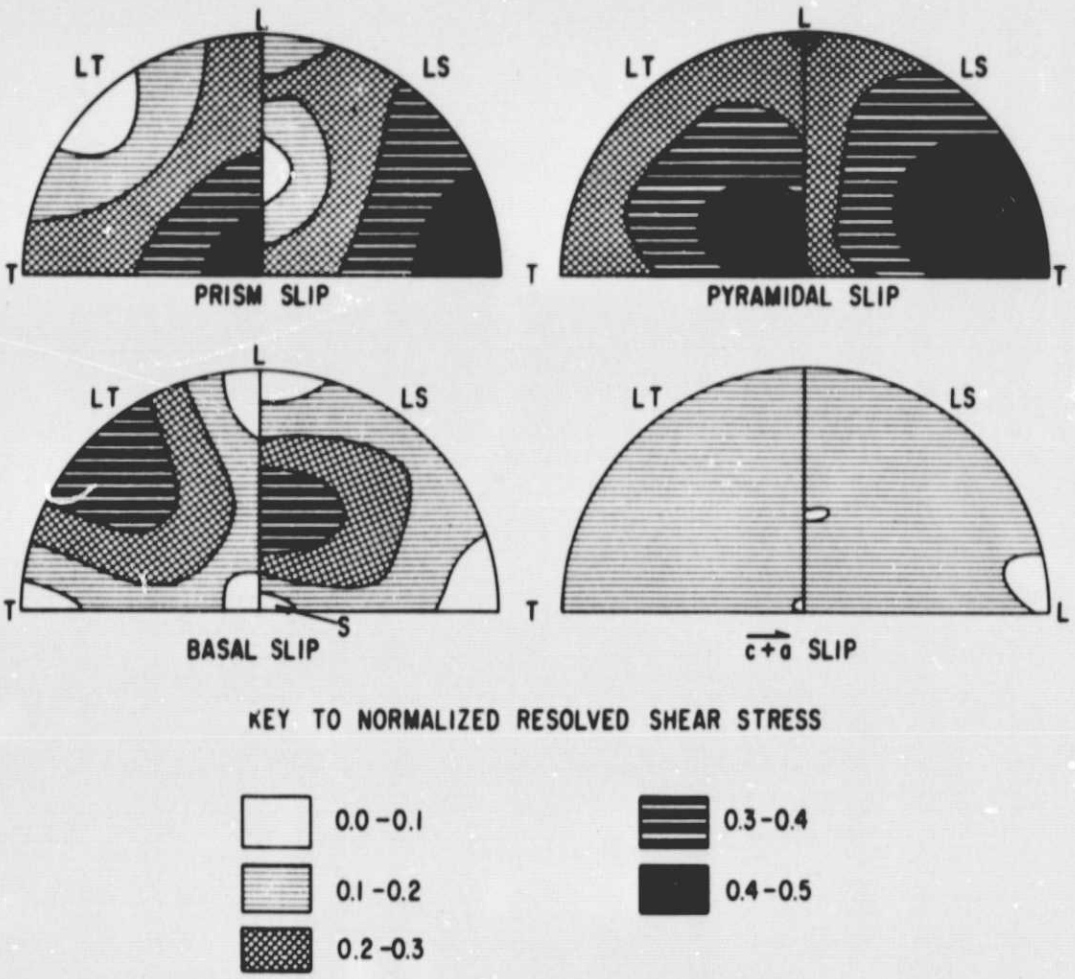

Figure B-1: Stereographic Projections Showing the Variation of Normalized Resolved Shear Stress for Slip in LS and LT Orientation Fracture Toughness Specimens. L, T, and S indicate longitudinal, transverse, and short transverse plate directions, respectively.

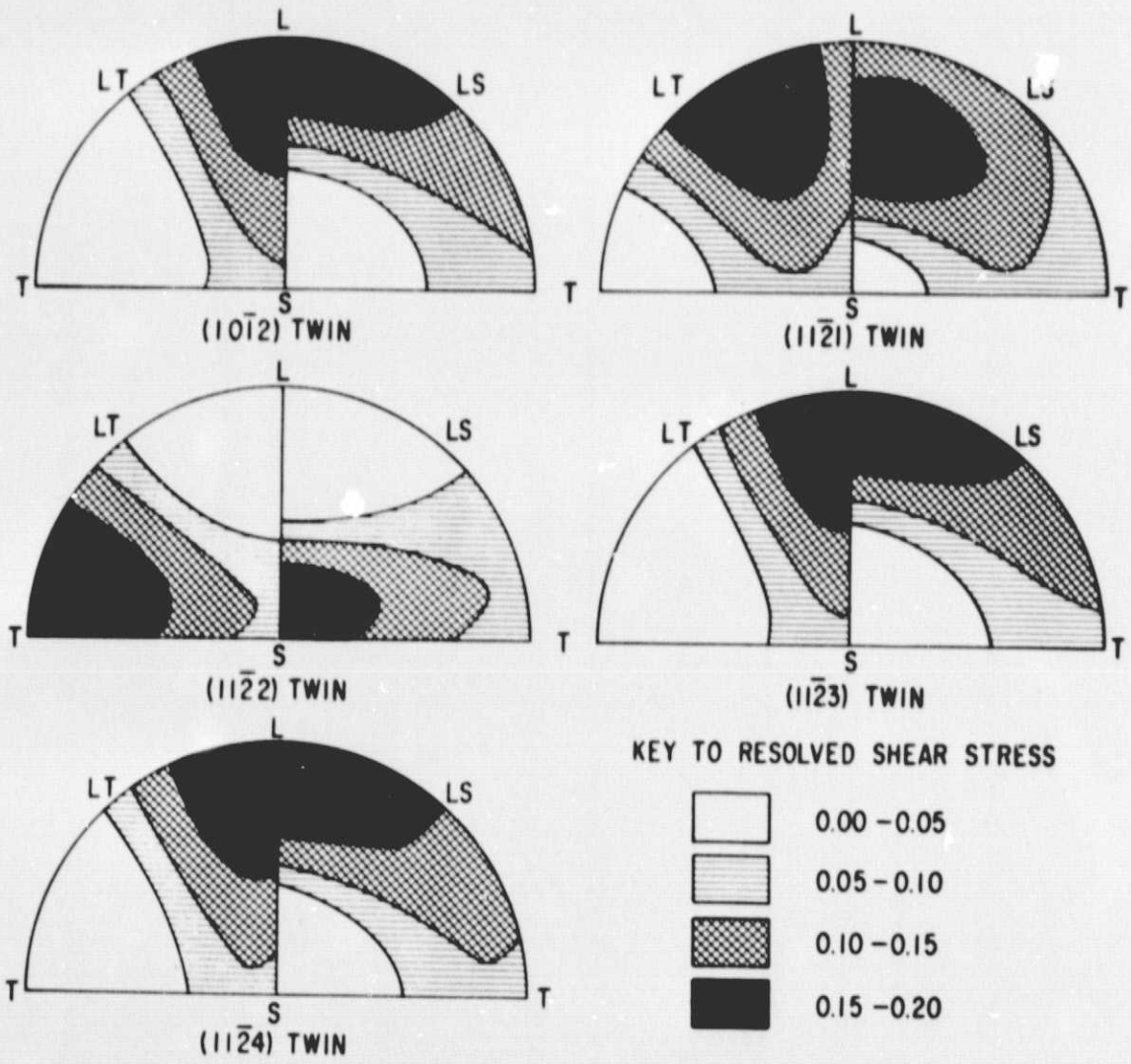

Figure B-2: Stereographic Projections Showing the Variation of Resolved Shear Stress for Twinning in LS and LT Orientation Fracture Toughness Specimens. L, T, and S indicate longitudinal, transverse, and short transverse plate directions, respectively.